10-30-2009

The White Dwarfs Within 20 Parsecs of the Sun: Kinematics and Statistics

Edward M. Sion
Villanova University

J. B. Holberg
University of Arizona

Terry D. Oswalt
Florida Institute of Technology, oswaltt1@erau.edu

George P. McCook
Villanova University

Richard Wasatonic
Villanova University

The Astronomical Journal, 138:1681–1689, 2009 December doi:10.1088/0004-6256/138/6/1681

THE WHITE DWARFS WITHIN 20 PARSECS OF THE SUN: KINEMATICS AND STATISTICS

Edward M. Sion[1], J. B. Holberg[2], Terry D. Oswalt[3], George P. McCook[1], and Richard Wasatonic[1]
[1] Department of Astronomy & Astrophysics, Villanova University, Villanova, PA 19085, USA; edward.sion@villanova.edu, george.mccook@villanova.edu, richard.wasatonic@villanova.edu
[2] Lunar and Planetary Laboratory, University of Arizona, Tucson, AZ 75201, USA; holberg@vega.lpl.arizona.edu
[3] Department of Physics and Space Sciences, Florida Institute of Technology, Melbourne, FL 32901, USA; toswalt@fit.edu
Received 2009 March 17; accepted 2009 September 15; published 2009 October 30

ABSTRACT

We present the kinematical properties, distribution of spectroscopic subtypes, and stellar population subcomponents of the white dwarfs within 20 pc of the Sun. We find no convincing evidence of halo white dwarfs in the total 20 pc sample of 129 white dwarfs nor is there convincing evidence of genuine thick disk subcomponent members within 20 parsecs. Virtually, the entire 20 pc sample likely belongs to the thin disk. The total DA to non-DA ratio of the 20 pc sample is 1.6, a manifestation of deepening envelope convection which transforms DA stars with sufficiently thin H surface layers into non-DAs. The addition of five new stars to the 20 pc sample yields a revised local space density of white dwarfs of $(4.9 \pm 0.5) \times 10^{-3}$ pc^{-3} and a corresponding mass density of $(3.3 \pm 0.3) \times 10^{-3}$ $M_{\odot}$ pc^{-3}. We find that at least 15% of the white dwarfs within 20 parsecs of the Sun (the DAZ and DZ stars) have photospheric metals that possibly originate from accretion of circumstellar material (debris disks) around them. If this interpretation is correct, this suggests the possibility that the same percentage have planets or asteroid-like bodies orbiting them.

Key words: stars: kinematics – stars: statistics – techniques: photometric – techniques: spectroscopic – white dwarfs

1. INTRODUCTION

The population of local white dwarfs (WDs) is astrophysically important for a number of reasons. First, from complete samples, it offers an excellent probe of the coolest, least luminous (oldest) component of the overall white dwarf population. Second, it samples the mix of stellar populations that evolve into the different spectroscopic subtypes in the immediate vicinity of the Sun. Third, it provides a unique way of measuring the local space density and mass density of white dwarfs which are currently of critical interest because: (1) they represent a history of star formation and stellar evolution in the Galactic plane; (2) the luminosity function of these stars can be used to place a lower limit on the age of the Galactic disk (Liebert 1988; Oswalt et al. 1996); (3) cool white dwarfs have been suggested as the origin of the MACHO lensing objects seen in lensing surveys (Oppenheimer et al. 2001; Kawaler 1996); and (4) they are important to understanding the overall mass density of the Galactic plane (Bahcall 1984).

Recently, Holberg et al. (2008, hereafter, LS08) completed a detailed survey of the local population of white dwarfs lying within 20 pc of the Sun which they estimated to be 80% complete. Their sample contained 124 individual degenerate stars, including both members of four unresolved double degenerate binaries, one of which was a suspected new double degenerate binary (WD0423+120). Since the publication of LS08, we have added seven additional white dwarfs to the 20 pc sample, bringing the present total to 131 degenerate stars. Two of these additional stars are close Sirius-like companions to nearby K stars (Holberg 2009), GJ86 (WD0208−510), and HD27442 (WD0415−594), discovered during exoplanet investigations (see Mugrauer & Neuhäuser 2005 and Chauvin et al. 2007, respectively). Of the remaining five single white dwarfs, three stars, WD0011−721, WD0708−670, and WD1116−470, are from Subasavage et al. (2008), and one star, WD1315−781, is from Subasavage et al. (2009). We have excluded one interesting high-velocity star, WD1339−340. Lepine et al. (2005) noted that this star had a space motion of 313 km s^{-1} relative to the Sun based on an assumed distance of 18 pc. Holberg et al. (2008) determined that WD1339−340 has an estimated distance of 21.2 ± 3.5 pc placing it formally outside the limits of our 20 pc sample. Nevertheless, this star has a finite probability of being within 20 pc.

Including the new stars in the local sample of 129 white dwarfs within 20 pc, yields a revised white dwarf space density of $(4.9 \pm 0.5) \times 10^{-3}$ pc^{-3}. The corresponding mass density is $(3.3 \pm 0.3) \times 10^{-3}$ $M_{\odot}$ pc^{-3}. The completeness of the sample, however, remains at 80% since the addition of the companion of GJ86 (at 10.8 pc) contributes to the number of white dwarfs within 13 pc upon which the stellar density is based.

In this work, we use the enlarged local sample to examine the kinematical properties, distribution of spectroscopic subtypes, and stellar population subcomponents of the white dwarfs sampled in this volume of space around the Sun.

2. DISTRIBUTION OF SPECTROSCOPIC SUBTYPES IN THE LOCAL WHITE DWARF POPULATION

Table 1 presents the sample of white dwarfs within 20 pc of the Sun. The basic observational data from which space motions have been computed are given in Table 1, which contains by column: (1) the WD number; (2) the coordinates (R.A. and decl. are in decimal degrees); (3) DIST (distance in parsecs); (4) PM (proper motion in arcsec yr^{-1}); (5) P.A. (position angle in degrees); and (6) the method of distance determination, denoted by *p* for trigonometric parallax, *s* for spectrophotometric distances, and *a* for a weighted average of the parallax and photometric distances according to their respective uncertainties. Distance estimates are taken from LS08 which are based on both trigonometric parallaxes and spectrophotometric distances. Whenever possible, preference was given to trigonometric parallax distances. In LS08, the photometric distances were computed based upon spectroscopic and photometric measurements using the techniques described in Holberg et al. (2008).

Table 1
Observational Data Used in Space Motions

WD	Type	R.A.	Decl.	DIST	PM	P.A.	Method
0000−345	DCP9	000.677	−34.225	12.65	0.899	217.337	a
0008+423	DA6.8	002.842	+42.668	17.94	0.237	193.4	s
0009+501	DAH7.7	002.413	+50.428	11.03	0.718	216.0	p
0011−134	DCH8.4	003.554	−13.177	19.49	0.911	217.7	p
0011−721	DA8.0	003.457	−71.831	17.80	0.326	141.300	s
0038−226	DQ9.3	010.354	−22.347	09.88	0.567	229.004	p
0046+051	DZ8.1	012.291	+05.388	04.32	2.978	155.538	p
0108+277	DAZ9.6	017.686	+27.970	13.79	0.227	219.321	s
0115+159	DQ6	019.500	+16.172	15.41	0.648	181.805	p
0121−429	DAH7.9	021.016	−42.773	17.67	0.540	155.143	p
0135−052	DA6.9	024.497	−04.995	12.35	0.681	120.838	p
0141−675	DA7.8	025.750	−67.282	09.70	1.048	198.279	s
0148+467	DA3.8	028.012	+47.001	16.06	0.124	000.568	a
0148+641	DA5.6	027.966	+64.431	17.13	0.285	123.857	s
0208+396	DAZ7.0	032.836	+39.922	16.13	1.145	115.746	a
0208−510	DA10	032.500	−50.133	10.8	2.192	72.666	p
0213+427	DA9.4	034.281	+42.977	19.67	1.047	125.065	a
0230−144	DC9.5	038.157	−14.197	15.38	0.687	177.114	a
0233−242	DC9.3	038.840	−24.013	15.67	0.622	189.015	s
0245+541	DAZ9.7	042.151	+54.383	10.35	0.573	227.827	p
0310−688	DA3.1	047.628	−68.600	10.15	0.111	158.097	p
0322−019	DAZ9.7	051.296	−01.820	16.81	0.909	164.625	p
0326−273	DA5.4	052.203	−27.317	19.73	0.850	071.629	s
0341+182	DQ7.7	056.145	+18.436	19.01	1.199	150.771	p
0344+014	DQ9.9	056.778	+01.646	19.90	0.473	150.400	s
0357+081	DC9.2	060.111	+08.235	17.46	0.535	222.273	a
0413−077	DAP3.1	063.839	−07.656	05.04	4.088	213.216	p
0415−594	DA3.8	064.122	−59.302	18.23	0.174	195.838	p
0423+120	DA8.2	066.473	+12.196	17.36	0.244	335.866	p
0426+588	DC7.1	067.802	+58.978	05.53	2.426	147.602	p
0433+270	DA9.3	069.187	+27.164	17.85	0.276	124.196	p
0435−088	DQ8.0	069.447	−08.819	09.51	1.574	171.103	p
0457−004	DA4.7	074.930	−00.377	17.67	0.293	142.872	s
0548−001	DQP8.3	087.831	−00.172	11.07	0.251	025.810	p
0552−041	DZ11.8	088.789	−04.168	06.45	2.376	166.966	p
0553+053	DAP8.9	089.106	+05.536	07.99	1.027	204.993	p
0642−166	DA2	101.288	−16.713	02.63	1.339	204.057	p
0644+025	DA8	101.789	+02.517	17.83	0.423	272.571	a
0644+375	DA2.5	101.842	+37.526	15.41	0.962	193.561	p
0655−390	DA8.0	104.274	−39.159	17.20	0.340	242.600	s
0657+320	DC10.1	105.215	+31.962	15.19	0.691	149.362	p
0659−063	DA7.8	105.478	−06.463	12.13	0.898	184.980	a
0708−670	DC	107.217	−67.108	17.50	0.246	246.300	s
0727+482.1	DA10.0	112.678	+48.199	11.01	1.286	190.069	a
0727+482.2	DA10.0	112.697	+48.173	11.20	1.286	190.069	a
0728+642	DAP11.2	113.378	+64.157	13.40	0.266	171.352	s
0736+053	DQZ6.5	114.827	+05.227	03.50	1.259	214.574	p
0738−172	DAZ6.7	115.086	−17.413	09.28	1.267	115.137	p
0743−336	DC10.6	116.396	−34.176	15.20	1.736	352.670	p
0747+073.1	DC12.1	117.563	+07.193	18.25	1.804	173.414	a
0747+073.2	DC11.9	117.563	+07.193	18.25	1.804	173.414	a
0749+426	DC11.7	118.305	+42.500	19.74	0.420	165.845	s
0751−252	DA10.0	118.485	−25.400	18.17	0.426	300.200	p
0752−676	DC10.3	118.284	−67.792	07.05	2.149	135.866	a
0806−661	DQ4.2	121.723	−66.304	19.17	0.398	132.700	p
0821−669	DA9.8	125.361	−67.055	10.65	0.758	327.600	p
0839−327	DA5.3	130.385	−32.943	08.07	1.600	322.056	a
0840−136	DZ10.3	130.701	−13.786	19.30	0.272	263.000	s
0912+536	DCP7	138.983	+53.423	10.31	1.563	223.997	p
0955+247	DA5.8	149.451	+24.548	18.83	0.420	219.848	s
1009−184	DZ7.8	153.007	−18.725	18.00	0.519	268.200	p
1019+637	DA7.3	155.787	+63.461	13.93	0.379	053.160	s
1033+714	DC9	159.260	+71.182	20.00	1.917	256.008	s
1036−204	DQP10.2	159.731	−20.682	14.29	0.628	333.300	p
1043−188	DQ8.1	161.412	−19.114	17.57	1.978	251.636	a
1055−072	DA6.8	164.396	−07.523	11.96	0.827	276.328	a

Table 1
(Continued)

WD	Type	R.A.	Decl.	DIST	PM	P.A.	Method
1116−470	DC	169.613	−47.365	17.90	0.322	275.100	s
1121+216	DA6.7	171.054	+21.359	13.55	1.040	269.240	a
1124+595	DA4.8	171.171	+59.321	17.90	0.156	108.203	s
1132−325	DC	173.623	−32.832	09.54	0.940	038.954	p
1134+300	DA2.5	174.271	+29.799	15.37	0.148	267.948	a
1142−645	DQ6.4	176.428	−64.841	04.62	2.687	097.414	p
1202−232	DAZ5.8	181.361	−23.553	10.82	0.229	009.068	p
1223−659	DA6.5	186.625	−66.205	16.25	0.153	195.124	p
1236−495	DA4.4	189.708	−49.800	13.71	0.490	255.708	a
1257+037	DA8.7	195.037	+03.478	16.18	0.969	206.195	a
1309+853	DAP9	197.171	+85.041	18.05	0.321	140.811	p
1310−472	DC11.9	198.248	−47.468	14.95	2.204	105.252	a
1315−781	DA	119.857	−78.239	19.23	0.470	139.5	p
1327−083	DA3.7	202.556	−08.574	16.47	1.204	246.761	a
1334+039	DZ10.0	204.132	+03.679	08.24	3.880	252.774	p
1344+106	DAZ7.1	206.851	+10.360	19.50	0.903	260.569	a
1345+238	DA10.7	207.125	+23.579	12.06	1.496	274.636	p
1444−174	DC10.1	221.855	−17.704	14.07	1.144	252.643	a
1544−377	DA4.7	236.875	−37.918	13.16	0.468	242.838	s
1609+135	DA5.8	242.856	+13.371	18.35	0.551	178.513	p
1620−391	DA2	245.890	−39.918	12.87	0.075	089.962	p
1626+368	DZ5.5	247.104	+36.771	15.95	0.888	326.667	p
1632+177	DA5	248.674	+17.609	15.99	0.088	108.434	s
1633+433	DAZ7.7	248.755	+43.293	15.11	0.373	144.151	p
1633+572	DQ8.2	248.589	+57.169	14.45	1.644	317.229	p
1647+591	DAV4.2	252.106	+59.056	10.79	0.323	154.498	a
1653+385	DAZ8.8	253.690	+38.493	15.35	0.328	177.596	s
1655+215	DA5.4	254.291	+21.446	18.63	0.582	178.040	a
1705+030	DZ7.1	257.033	+02.962	17.54	0.379	180.907	p
1748+708	DQP9.0	267.033	+70.876	06.07	1.681	311.394	p
1756+827	DA7.1	270.359	+82.745	15.55	3.589	336.541	a
1814+134	DA9.5	274.277	+13.473	14.22	1.207	201.500	p
1820+609	DA10.5	275.332	+61.018	12.79	0.713	168.516	p
1829+547	DQP7.5	277.584	+54.790	14.97	0.399	317.233	p
1900+705	DAP4.5	285.042	+70.664	12.99	0.506	010.466	p
1917+386	DC7.9	289.744	+38.722	11.70	0.251	174.028	p
1917−077	DBQA5	290.145	−07.666	10.08	0.174	200.602	p
1919+145	DA3.5	290.417	+14.673	19.80	0.074	203.805	p
1935+276	DA4.5	294.307	+27.721	18.00	0.436	088.686	a
1953−011	DAP6.5	299.121	−01.042	11.39	0.827	212.314	p
2002−110	DA10.5	301.395	−10.948	17.33	1.074	095.523	p
2007−303	DA3.3	302.736	−30.218	15.37	0.428	233.492	p
2008−600	DC9.9	303.132	−59.947	16.55	1.440	165.500	p
2032+248	DA2.5	308.591	+25.063	15.65	0.692	215.554	a
2047+372	DA4	312.277	+37.470	17.77	0.219	047.150	s
2048+263	DA9.7	312.586	+26.511	19.89	0.514	235.044	a
2054−050	DC10.9	314.199	−04.844	17.06	0.802	106.562	p
2105−820	DAP4.9	318.320	−81.820	18.12	0.516	146.371	a
2117+539	DA3.5	319.734	+54.211	17.88	0.213	336.371	a
2138−332	DZ7	325.489	−33.008	15.63	0.210	228.500	
2140+207	DQ6.1	325.670	+20.999	12.52	0.681	199.444	p
2154−512	DQ7	329.410	−51.008	16.36	0.374	184.738	p
2159−754	DA5	331.087	−75.223	14.24	0.529	275.635	s
2211−392	DA8	333.644	−38.985	18.80	1.056	110.100	p
2226−754	DC9.9	337.662	−75.232	15.11	1.868	167.500	s
2226−755	DC12.1	337.639	−75.256	15.11	1.868	167.500	s
2246+223	DA4.7	342.273	+22.608	19.05	0.525	083.551	p
2251−070	DZ13	343.472	−06.781	08.08	2.585	105.369	p
2322+137	DA10.7	351.332	+14.060	18.76	0.037	071.565	s
2326+049	DAZ4.4	352.198	+05.248	13.62	0.493	236.406	p
2336−079	DAZ4.6	354.711	−07.688	15.94	0.192	172.208	p
2341+322	DA4.0	355.961	+32.546	18.33	0.229	252.150	a
2359−434	DAP5.8	000.544	−43.165	07.27	1.020	135.198	p

Note. s: spectrophotometric, p: trigonometric parallax, a: weighted mean average.

Table 2
Distribution of WD Spectral Subtypes within 20 Parsecs

Spectral Type	Number of Stars	% of Total
DP, DH	17	13%
DA	58	45%
DAZ	11	8%
DZ	9	7%
DQ	12	9%
DC	21	16%
DBQZ	1	1%

Proper motions are taken from the McCook and Sion Catalog, or where available, were determined from NOMAD. Radial velocities were available from the literature for approximately 50% of our sample, and correspond either to direct measurements of the white dwarf or the system velocities or radial velocities of the main-sequence companions. For radial velocities derived from individual white dwarfs, corrections for the gravitational redshift have been made based on the individual masses and radii of each star. These mass and radius determinations were interpolated from within the synthetic photometric tables described in Holberg & Bergeron (2006) and were based on temperatures and gravities given in LS08.

Using the spectral types given in LS08 and revised by Holberg (2009), we summarize the percentage breakdown of spectral subtypes among the 20 pc sample of local white dwarfs in Table 2. As expected, the DA stars dominate the sample with the other spectral groups having roughly the same percentages as the proper-motion-selected white dwarf sample as a whole.

The DAZ stars which exhibit photospheric metal lines due to accreted metals are counted separately from the "pure" DA stars in the 20 pc sample. The 11 DAZ stars within 20 pc account for 8% of the local sample while the DZ stars, which have helium-rich atmospheres account for 7% of the 20 pc sample. There is only one DB star within 20 parsecs, the cool DBQZ star LDS678A while the DQ stars, which exhibit molecular and atomic carbon, account for 9%.

The value of the total DA to non-DA ratio of the 20 pc sample, obtained here, is 1.6. This ratio holds important astrophysical significance since the competition between accretion, diffusion, and convective mixing controls and/or modifies the flow of elements in a high gravity atmosphere and hence determines what elements are spectroscopically detected at the surface (Strittmatter & Wickramasinghe 1971). The value of the ratio obtained here is expected for a sample dominated by cool degenerates since earlier observational studies showed that there is a gradual reduction of this ratio from 4:1 for white dwarfs hotter than 20,000 K down to roughly 1:1 for the coolest degenerates below 10,000 K (Sion 1984; Greenstein 1986). This transformation in the DA/non-DA ratio occurs when mixing by deepening envelope convection increasingly transforms DA white dwarfs with sufficiently thin surface H layers into non-DA stars (Sion 1984; Greenstein 1986, and references therein). However, DA stars begin their cooling evolution with a range of hydrogen layer masses. Those with thick hydrogen layers may not transform via convective mixing and dilution and will remain DA until the Balmer lines fade below 5000 K while DA stars with sufficiently thin hydrogen layers should undergo transformation to non-DA stars as the deepening H convection reaches the deeper, more massive underlying helium convection zone. Thus, some cooling DA stars may transform to DZ stars when the hydrogen is mixed downward and diluted by the deepening helium convection. Such an object would be classified DZA and may owe their observed H abundances to convective mixing and dilution instead of accretion.

3. KINEMATICS OF THE LOCAL WHITE DWARFS

For the local white dwarfs with sufficient kinematical information (photometric or trigonometric parallax, proper motion, position angle), we have computed the vector components of the space motion U, V, and W relative to the Sun in a right-handed system following Wooley et al. (1970) where U is measured positive in the direction of the Galactic anti-center, V is measured positive in the direction of the Galactic rotation, and W is measured positive in the direction of the north Galactic pole.

The space motions were calculated in two ways: (1) using any known radial velocities for 55 of the 129 stars in the 20 pc sample and (2) by assuming zero radial velocity for the entire sample. Also calculated were the average velocity, velocity dispersions, and standard errors for the entire sample of 129 WDs and for each spectroscopic subclass separately. We found relatively little kinematical difference among the samples if we used the 55 available radial velocities and the sample with the assumption of zero radial velocity. This finding is consistent with earlier studies (Silvestri et al. 2002; Pauli et al. 2003, 2006) which reported little difference in the kinematical results with or without the inclusion of radial velocities.

Table 3 lists by column: the WD number, the white dwarf spectral type, U-component, V-component, W-component, and T, the total space velocity. All velocities are expressed in km s^{-1}. At the end of the tabulation of individual white dwarf motions, we have listed the average velocity in each of the three vector components and in the total motion, T, for the white dwarfs within 20 pc, the velocity dispersion in each average velocity component, and the standard error in each velocity component.

In order to try to assign stellar population membership, it is useful to compare the distribution of space velocities of the 20 parsec sample with other analyses in which the assignment of population membership is on a secure footing. Since the population membership of main-sequence stars, unlike white dwarfs, is assigned with chemical abundance data as well as kinematical characteristics, it is illuminating to compare the distribution of white dwarfs in the UV velocity plane for the 20 pc sample with the velocity distribution (velocity ellipses) of a well-studied sample of main-sequence stars. In Figure 1, we have displayed the U versus V space velocity diagram for the 20 pc sample of white dwarfs with the assumption of zero radial velocity relative to three velocity ellipses for main-sequence stars (Chiba & Beers 2000; see also Kawka & Vennes 2006). In the diagram, we have displayed the 2σ velocity ellipse contour (solid line) of the thin disk component, the 2σ ellipse of the thick disk component (short-dashed line), and the 1σ contour of the halo component (long-dashed line).

Examining Table 3, if we take $T > 150$ km s^{-1} as the lower cutoff for halo space motions, then at first glance, six stars or 4% of the total sample could be considered likely candidates for the halo population subcomponent. However, the assignment of white dwarfs to the halo population subcomponent cannot be made on the basis of space motions alone. The candidate white dwarfs must also have total stellar ages that are of order 12 billion years or older. In Table 4, we have tabulated the cooling ages of the white dwarfs in the 20 pc sample in descending order of decreasing age. The cooling ages listed in Table 4 have been interpolated from the photometric grid of P. Bergeron[4]. Hence,

[4] http://www.astro.umontreal.ca/~bergeron/CoolingModels/

Table 3
Space Motions of White Dwarfs Within 20 pc

WD No.	Type	*U*	*V*	*W*	*T*
0000−345	DCP9	−11.9	−43.7	3.2	45.4
0008+423	DA6.8	−10.0	−1.9	−17.4	20.2
0009+501	DAH7.7	−28.1	8.6	−24.1	38.0
0011−134	DCH8.4	−75.5	−31.1	−9.8	82.3
0011−721	DA8.0	10.3	−23.2	12.2	28.2
0038−226	DQ9.3	−24.9	−4.6	−1.2	25.3
0046+051	DZ8.1	−2.8	−53.6	−30.3	61.6
0108+277	DAZ9.6	−11.9	0.3	−9.9	15.5
0115+159	DQ6	−21.4	−27.2	−32.0	47.2
0121−429	DAH7.9	−0.7	−46.8	11.1	48.1
0135−052	DA6.9	16.8	−37.2	−1.6	40.9
0141−675	DA7.8	−21.8	−22.8	21.5	38.2
0148+467	DA3.8	2.6	1.8	8.3	8.8
0148+641	DA5.6	12.3	−11.2	−6.8	18.0
0208+396	DAZ7.0	43.0	−62.9	−6.7	76.5
0208−510	DA10	85.6	−42.1	24.0	98.4
0213+427	DA9.4	37.8	−67.3	−19.8	79.8
0230−144	DC9.5	−20.7	−43.3	−13.3	49.9
0233−242	DC9.3	−24.2	−34.1	−9.8	43.0
0245+541	DAZ9.7	−16.4	10.9	−24.2	31.3
0310−688	DA3.1	0.1	−4.2	2.8	5.1
0322−019	DAZ9.7	−21.5	−66.8	−20.7	73.2
0326−273	DA5.4	46.7	−29.7	47.2	72.8
0341+182	DQ7.7	−16.0	−94.9	−23.8	99.1
0344+014	DQ9.9	−7.9	−43.8	−4.9	44.8
0357+081	DC9.2	−25.3	−4.3	−36.8	44.9
0413−077	DAP3.1	−44.2	−34.8	−73.0	92.2
0415−594	DA3.8	−4.9	−5.7	−1.6	7.7
0423+120	DA8.2	5.3	18.1	3.8	19.3
0426+588	DC7.1	0.9	−35.4	−3.7	35.6
0433+270	DA9.3	−0.1	−19.8	7.0	21.1
0435−088	DQ8.0	−25.1	−63.2	−21.6	71.4
0457−004	DA4.7	−6.1	−23.8	2.5	24.7
0548−001	DQP8.3	4.6	6.3	10.5	13.1
0552−041	DZ11.8	−25.3	−65.7	−20.2	73.3
0553+053	DAP8.9	−12.2	−19.8	−31.2	38.9
0642−166	DA2	−0.6	−10.2	−14.5	17.7
0644+025	DA8	9.4	15.1	−30.9	35.7
0644+375	DA2.5	−19.7	−39.6	−32.7	55.1
0655−390	DA8.0	2.7	2.3	−28.2	28.4
0657+320	DC10.1	−23.3	−40.0	10.4	47.5
0659−063	DA7.8	−19.7	−37.5	−29.5	51.6
0708−670	DC	4.7	4.9	−19.9	21.1
0727+482.1	DA10.0	−14.6	−40.5	−14.7	45.5
0727+482.2	DA10.0	−14.9	−41.1	−14.9	46.3
0728+642	DAP11.2	−4.5	−9.2	3.9	11.0
0736+053	DQZ6.5	0.6	−12.0	−18.4	21.9
0738−172	DAZ6.7	−30.5	−29.2	30.2	51.9
0743−336	DC10.6	49.4	67.6	61.4	103.9
0747+073.1	DC12.1	−76.7	−126.3	−49.0	155.7
0747+073.2	DC11.9	−76.7	−126.3	−49.0	155.7
0749+426	DC11.7	−17.8	−29.6	5.6	35.0
0751−252	DA10.0	19.1	15.5	−13.8	28.3
0752−676	DC10.3	−29.3	−15.4	13.6	35.9
0806−661	DQ4.2	−17.2	−6.5	7.3	19.8
0821−669	DA9.8	16.8	4.5	4.4	18.0
0839−327	DA5.3	38.2	26.6	4.6	46.8
0840−136	DZ10.3	14.0	−0.0	−21.0	25.2
0912+536	DCP7	21.0	−42.5	−24.3	53.3
0955+247	DA5.8	6.1	−28.1	−17.7	33.8
1009−184	DZ7.8	36.1	−8.8	−26.4	45.6
1019+637	DA7.3	−14.7	17.9	3.5	23.4
1033+714	DC9	138.8	−73.2	−58.0	167.3
1036−204	DQP10.2	36.0	17.9	20.7	45.2
1043−188	DQ8.1	110.7	−71.1	−107.8	170.1
1055−072	DA6.8	42.3	−10.4	−16.3	46.5
1116−470	DC	24.3	−9.2	−7.0	27.0
1121+216	DA6.7	57.8	−25.3	−21.5	66.7
1124+595	DA4.8	−12.2	1.3	6.0	13.7
1132−325	DC	−11.4	22.5	35.8	43.8
1134+300	DA2.5	9.2	−4.6	−2.9	10.7
1142−645	DQ6.4	−52.1	25.3	6.6	58.3
1202−232	DAZ5.8	3.0	6.1	8.6	11.0
1223−659	DA6.5	0.7	0.1	−8.4	8.4
1236−495	DA4.4	24.0	−17.0	−8.6	30.7
1257+037	DA8.7	−6.2	−69.4	−25.6	74.2
1309+853	DAP9	−16.3	−1.3	15.4	22.5
1310−472	DC11.9	−133.6	81.4	−51.5	164.8
1315−781	DA	−23.5	+26.4	−32.3	47.8
1327−083	DA3.7	49.2	−76.6	−7.4	91.3
1334+039	DZ10.0	87.5	−122.2	8.5	150.5
1344+106	DAZ7.1	54.6	−62.3	14.1	84.1
1345+238	DA10.7	67.0	−47.4	20.1	84.5
1444−174	DC10.1	33.0	−61.4	17.6	71.9
1544−377	DA4.7	5.5	−22.4	7.6	24.3
1609+135	DA5.8	−25.2	−35.3	−17.4	46.8
1620−391	DA2	−1.3	2.8	−3.2	4.5
1626+368	DZ5.5	35.1	15.5	35.6	52.3
1632+177	DA5	−2.7	2.3	−5.3	6.4
1633+433	DAZ7.7	−12.7	−4.2	−13.9	19.4
1633+572	DQ8.2	45.4	−3.0	54.5	71.0
1647+591	DAV4.2	−6.0	−3.0	−5.4	8.6
1653+385	DAZ8.8	−10.4	−14.8	−5.5	18.9
1655+215	DA5.4	−25.9	−35.9	−18.4	47.9
1705+030	DZ7.1	−16.6	−23.1	−13.4	31.5
1748+708	DQP9.0	5.8	−10.8	34.2	36.3
1756+827	DA7.1	8.8	−30.3	106.4	111.0
1814+134	DA9.5	−47.7	−72.0	−8.6	86.8
1820+609	DA10.5	−9.8	−9.0	−19.7	23.7
1829+547	DQP7.5	2.8	−0.7	24.3	24.4
1900+705	DAP4.5	6.7	5.5	6.0	10.5
1917+386	DC7.9	−5.2	−5.7	−8.6	11.6
1917−077	DBQA5	−5.4	−6.4	−0.5	8.4
1919+145	DA3.5	−4.2	−5.0	−0.7	6.6
1935+276	DA4.5	16.0	10.2	−31.7	37.0
1953−011	DAP6.5	−32.3	−31.9	3.7	45.6
2002−110	DA10.5	40.4	9.8	−76.6	87.2
2007−303	DA3.3	−22.0	−18.3	18.0	33.8
2008−600	DC9.9	−17.7	−62.3	−3.3	64.9
2032+248	DA2.5	−36.9	−24.9	−2.8	44.7
2047+372	DA4	13.4	5.5	−1.4	14.6
2048+263	DA9.7	−37.6	−16.2	11.8	42.7
2054−050	DC10.9	31.1	−11.4	−54.1	63.5
2105−820	DAP4.9	12.5	−17.4	3.6	21.8
2117+539	DA3.5	−0.8	2.1	18.3	18.5
2138−332	DZ7	−15.0	−8.3	8.4	19.1
2140+207	DQ6.1	−28.0	−18.9	−17.1	37.9
2154−512	DQ7	−12.4	−22.4	9.9	27.5
2159−754	DA5	−27.6	7.6	18.5	34.1
2211−392	DA8	57.8	−43.7	−44.5	85.1
2226−754	DC9.9	−0.5	−88.5	71.5	113.8
2226−755	DC12.1	−0.5	−88.5	71.5	113.8
2246+223	DA4.7	42.4	−10.4	−16.9	46.8
2251−070	DZ13	68.0	−48.2	−50.0	97.2
2322+137	DA10.7	3.2	−0.5	−0.3	3.2
2326+049	DAZ4.4	−31.6	−2.1	−1.3	31.7
2336−079	DAZ4.6	−5.8	−13.4	−5.9	15.8
2341+322	DA4.0	−18.8	5.6	−0.4	19.6
2359−434	DAP5.8	13.9	−16.4	−27.6	35.0
		U	*V*	*W*	*T*
Avg.		+0.9	−21.5	−5.2	47.6
Disp.		35.3	33.1	28.1	36.6
Error		3.1	2.9	2.4	3.2

Table 4
Cooling Ages of White Dwarfs Within 20 pc

WD No.	$T_{\rm eff}$	Log g	Age
WD2251−070	4000	8.01	9.04E+09
WD1310−472	4220	8.12	8.83E+09
WD2226−755	4177	8	8.54E+09
WD2226−754	4230	8	8.40E+09
WD0749+426	4300	8	8.19E+09
WD2002−110	4800	8.31	8.14E+09
WD1444−174	4960	8.37	8.03E+09
WD2054−050	4620	8.09	7.58E+09
WD0728+642	4500	8	7.58E+09
WD0108+277	5270	8.36	6.93E+09
WD0208−510	4700	8	6.90E+09
WD0747+073.1	4850	8.04	6.53E+09
WD0743−336	4740	7.97	6.52E+09
WD0552−041	4270	7.8	6.42E+09
WD0747+073.2	5000	8.12	6.41E+09
WD0245+541	5280	8.28	6.30E+09
WD1033+714	4888	8	6.15E+09
WD0657+320	4990	8.07	6.15E+09
WD0727+482.2	5060	8.12	6.13E+09
WD0840−136	4900	8	6.10E+09
WD1036−204	4948	8	5.90E+09
WD1748+708	5590	8.36	5.69E+09
WD2008−600	5078	8	5.28E+09
WD0344+014	5084	8	5.25E+09
WD1820+609	4780	7.83	5.24E+09
WD1345+238	4590	7.76	5.20E+09
WD1334+039	5030	7.95	5.19E+09
WD0708−670	5108	8	5.12E+09
WD0727+482.1	5020	7.92	5.03E+09
WD0751−252	5159	8	4.86E+09
WD0821−669	5160	8	4.86E+09
WD1829+547	6280	8.5	4.78E+09
WD1653+385	5700	8.28	4.77E+09
WD0659−063	6520	8.71	4.40E+09
WD0752−676	5730	8.21	4.19E+09
WD1257+037	5595	8.16	4.18E+09
WD0230−144	5480	8.11	4.12E+09
WD1814+134	5313	8	4.09E+09
WD0553+053	5790	8.2	3.97E+09
WD0433+270	5620	8.14	3.97E+09
WD0213+427	5600	8.12	3.87E+09
WD0000−345	6240	8.31	3.78E+09
WD0233−242	5400	8	3.66E+09
WD0009+501	6610	8.36	3.58E+09
WD0644+025	7410	8.66	3.48E+09
WD0011−134	6010	8.2	3.43E+09
WD1917+386	6390	8.28	3.42E+09
WD0357+081	5490	8.02	3.37E+09
WD0038−226	5400	7.91	3.29E+09
WD0548−001	6070	8.18	3.24E+09
WD0046+051	6220	8.19	3.13E+09
WD1055−072	7420	8.42	3.02E+09
WD1309+853	5600	8	2.98E+09
WD0008+423	7380	8.38	2.89E+09
WD1705+030	6580	8.2	2.80E+09
WD2159−754	9040	8.95	2.76E+09
WD1019+637	6981	8.253	2.69E+09
WD0912+536	7160	8.28	2.66E+09
WD1633+572	6180	8.09	2.60E+09
WD1043−188	6190	8.09	2.59E+09
WD1116−470	5856	8	2.50E+09
WD2359−434	8570	8.6	2.48E+09
WD0426+588	7120	8.17	2.21E+09
WD0423+120	6150	8	2.11E+09
WD1121+216	7471	8.197	2.08E+09
WD1609+135	9321	8.644	2.08E+09

Table 4
(Continued)

WD No.	$T_{\rm eff}$	Log g	Age
WD0141−675	6460	8.04	2.07E+09
WD0457−004	10800	9.15	2.02E+09
WD2211−392	6290	8	2.00E+09
WD1344+106	7135	8.119	1.97E+09
WD0121−429	6369	8	1.93E+09
WD1953−011	7920	8.23	1.91E+09
WD0655−390	6415	8	1.90E+09
WD0011−721	6439	8	1.88E+09
WD1009−184	6449	8	1.87E+09
WD0435−088	6300	7.93	1.87E+09
WD0341+182	6510	7.99	1.81E+09
WD2246+223	10647	8.803	1.79E+09
WD0322−019	5220	7.5	1.79E+09
WD0208+396	7340	8.1	1.77E+09
WD0955+247	8621	8.301	1.73E+09
WD2322+137	4700	7	1.73E+09
WD0148+641	8938	8.354	1.70E+09
WD1223−659	7740	8.13	1.66E+09
WD2048+263	5200	7.31	1.58E+09
WD0738−172	7590	8.07	1.51E+09
WD1236−495	11748	8.802	1.46E+09
WD2138−332	7188	8	1.43E+09
WD1633+433	6518	7.735	1.39E+09
WD1142−645	7900	8.07	1.36E+09
WD1756+827	7270	7.98	1.36E+09
WD0115+159	9050	8.19	1.24E+09
WD0135−052	7280	7.85	1.20E+09
WD0736+053	7740	8	1.18E+09
WD1655+215	9313	8.203	1.17E+09
WD1202−232	8774	8.1	1.11E+09
WD1626+368	8440	8.02	9.95E+08
WD1900+705	12070	8.58	9.48E+08
WD2140+207	8200	7.84	8.77E+08
WD2105−820	10559	8.184	7.67E+08
WD0839−327	9268	7.885	6.67E+08
WD0326−273	9250	7.86	6.55E+08
WD1544−377	10538	8.09	6.46E+08
WD1647+591	12260	8.31	6.06E+08
WD2336−079	11040	8.11	5.89E+08
WD1917−077	10200	8	5.74E+08
WD1632+177	10100	7.956	5.67E+08
WD1124+595	10500	8	5.31E+08
WD2326+049	11562	8.008	4.20E+08
WD1935+276	12130	8.05	4.05E+08
WD0806−661	11940	8	3.79E+08
WD2047+372	14070	8.21	3.61E+08
WD2341+322	12570	7.93	3.09E+08
WD0415−594	13342	8	2.80E+08
WD0148+467	13430	7.93	2.56E+08
WD1919+145	15108	8.078	2.31E+08
WD1327−083	13920	7.86	2.14E+08
WD1134+300	21276	8.545	1.93E+08
WD2117+539	13990	7.78	1.93E+08
WD2007−303	14454	7.857	1.90E+08
WD0310−688	15500	8.027	1.90E+08
WD0413−077	16176	7.865	1.33E+08
WD0642−166	25193	8.556	1.12E+08
WD0644+375	21060	8.1	8.12E+07
WD2032+248	19980	7.83	5.66E+07
WD1620−390	24276	8.011	3.01E+07

when we take into account the total stellar ages of each of the six stars in Table 3 with $T > 150$ km s^{-1}, then we conclude that based upon their space motions together with their total stellar

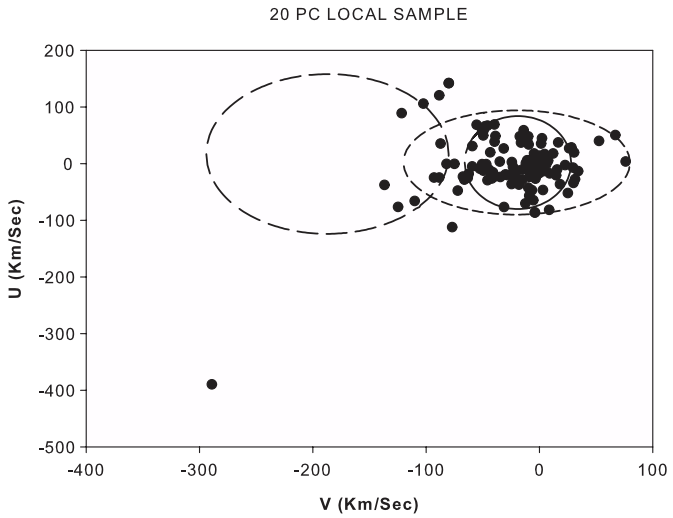

Figure 1. U vs. V space velocity diagram for the 20 pc sample of white dwarfs with the assumption of zero radial velocity. For comparison, three velocity ellipses for main-sequence stars are shown following Chiba & Beers (2000; see also Kawka & Vennes 2006), the 2σ velocity ellipse contour (solid line) of the thin disk component, the 2σ ellipse of the thick disk component (short-dashed line), and the 1σ contour of the halo component (long-dashed lines).

Table 5
Subgroup Velocity Statistics

Spectral Type	N	Component	Avg.	Disp.	Error
DA (DA+DAV+DAZ)	69	U	4.9	28.8	3.4
		V	−15.8	25.5	3.0
		W	−4.3	23.1	2.7
		T	39.0	27.6	3.2
Magnetics	17	U	−7.2	26.6	6.4
		V	−15.7	20.1	4.8
		W	−3.1	26.1	6.3
		T	39.0	22.6	5.4
DC	21	U	−8.6	53.0	11.5
		V	−32.0	53.6	11.7
		W	−3.6	39.7	8.6
		T	74.7	50.9	11.1
DQ	12	U	−4.0	42.7	12.3
		V	−28.5	33.9	9.7
		W	−12.3	37.7	10.8
		T	57.8	42.7	12.3
DZ	9	U	20.1	39.5	13.1
		V	−34.9	42.4	14.1
		W	−12.0	25.5	8.5
		T	61.8	41.3	13.7

ages, no clear evidence of halo white dwarfs has been found among the white dwarfs within 20 pc of the Sun.

If we take the range of total velocities $60 < T < 150$ km s^{-1} to be the range of space motions of the thick disk subcomponent and if we take total motions less than 60 km s^{-1} to be characteristic of the thin disk, then, at first glance, 28 white dwarfs (21% of the 20 pc sample) in Table 1 could potentially belong to the thick disk with the vast majority of stars (79%) belonging to the thin disk. However, distinguishing thin disk from thick disk members is a daunting task which involves far more than simply using space motions alone. Napiwotzki (2009) has already noted that it is not possible to uniquely identify thick disk stars from thin disk stars based on space motions in the U–V plane alone or even with all three vector components available. This is because the space motions of these thin and thick disk populations overlap. Napiwotzki (2006) used Monte Carlo simulations of the two populations to estimate the relative contribution of the two populations to his observed sample. Thus, in the range 60 km s^{-1} $< v \tan <$ 150 km s^{-1}, it is not possible to uniquely identify bona fide thick disk stars without considering their total stellar ages as well as applying a Galactic model as was done by Pauli et al. (2006). Star formation in the thick disk ended more than 10 billion years ago. It is clear that white dwarfs which are the descendants of the thick disk population should have large velocity dispersions similar to those given by Chiba & Beers (2000) for the thick disk while having lower than average masses since they are the descendants of low mass progenitors (Napiwotzki 2009). The velocity dispersions, $\sigma(U)$, $\sigma(V)$, and $\sigma(W)$ of the entire 20 pc sample lies below the boundary line for thick disk membership which is defined by Chiba & Beers (2000) to be $\sigma(U) =$ 46 km s^{-1}, $\sigma(V) = 50$ km s^{-1}, and $\sigma(W) = 35$ km s^{-1}.

This conclusion about the absence of genuine thick disk members in the 20 pc sample is supported by Silvestri et al.'s (2002) study of 116 common proper-motion binaries with white dwarf plus M dwarf components. Their wide binary pairs gave them at least three independent parameters related to stellar population subcomponent membership: (1) abundance; (2) intrinsic radial velocity; and (3) age (from chromospheric activity, main sequence fitting, etc.). They present kinematics plots (see their Figures 4 and 5) of their wide binary pairs which indicate by comparison with our Figure 1 that there are few, if any, halo or thick disk objects in the local 20 pc WD sample. Our local sample has a far smaller velocity dispersion than the Silvestri et al. (2002) sample.

Even in much larger samples of white dwarfs such as the Pauli et al. (2003, 2006) SN Ia Progenitor surveY (SPY), there are relatively few genuine halo and thick disk candidates. For example, in their sample of 398 white dwarfs which effectively constituted a magnitude-limited sample, they examined both the UVW space motions and the Galactic orbits of their stars. They found that only 2% of their sample kinematically belonged to the halo and 7% to the thick disk.

Other explanations for high-velocity white dwarfs exist. For example, Rappaport et al. (1994) and Davies et al. (2001) have shown that Type II supernovae may disrupt binaries with orbital periods in the range of 0.3–2 days, yielding single stars whose space velocities are similar to their original presupernova orbital velocities, $V_{\rm orb}$. Thus, a population of high-velocity white dwarfs can be expected to arise from within the thin disk component of the Galactic disk, at least from this mechanism. High-velocity stars may also arise from much wider binary pairs (see Kawka et al. 2006).

In Table 5, we have tabulated the velocity statistics broken down by spectral subgroup. By column is listed: (1) the spectroscopic subgroup; (2) N, the number of white dwarfs of a given spectral type; (3) the vector components of velocity U, V, and W and the total motion T; (4) the average velocity in each component; (5) the velocity dispersion of each component; and (6) the error in each component. The motions of individual spectroscopic subgroups, as seen in Table 5, differ little from each other although compared with the size of the DA sample, the non-DA groups are relatively small in number. The only subgroup of white dwarfs differing significantly at least from the non-DA subgroups are the magnetic white dwarfs, which have significantly lower space velocities. Here again, caution is advised because there are only 16 magnetic degenerates with known space motions within 20 parsecs of the Sun. Nonetheless,

the trend is in the direction expected from earlier kinematical evidence (Sion et al. 1988; Anselowitz et al. 1999) that they are the progeny of more massive stars. We find a smaller fraction of magnetic white dwarfs, 12%, of the 20 pc sample than Kawka & Vennes (2006) who found 20% magnetics within 13 pc of the Sun. However, given the quoted uncertainty in the percentage of magnetic degenerates in their sample and the lower completeness of the 20 pc sample, we cannot attach any significance to the differences at the present time.

Finally, although the number of stars in each non-DA spectroscopic subgroup may be too small for a statistically significant comparison, it appears that the magnetic white dwarfs have significantly lower velocities and velocity dispersions than the non-DA spectral types. However, magnetic white dwarfs closely resemble the kinematical properties of the DA white dwarfs within 20 pc.

4. DISCUSSION

We have attempted to fully characterize the white dwarfs within 20 pc of the Sun since LS08. By adding six new objects within 20 pc, there is now a total of 129 individual degenerate stars. Three of the added objects are from Subasavage et al. (2008), one object is from Subasavage et al. (2009), and two are in wide binaries (Holberg 2009). The completeness of the 20 pc sample remains at 80%. Based upon the sample of white dwarfs within 13 pc which is likely 100% complete, the local space density of white dwarfs has been revised to $(4.9 \pm 0.5) \times 10^{-3}$ pc^{-3}.

In this volume-limited sample, every major white dwarf spectral type (DA, DC, DQ, DZ, DH/DP) is found except for the pure DB and DO stars. There is, however, one cool, hybrid DB, the DBQZ star LDS678A within 20 pc. Based upon their individual space motions, velocity averages, velocity dispersions, and total stellar ages, the 20 pc sample of white dwarfs overwhelmingly consists of members of the thin disk population. There is no clear evidence of either halo population white dwarfs or bona fide thick disk members. It also appears that the magnetic white dwarfs have significantly lower velocities and lower velocity dispersions than the non-DA spectral types but similar velocity dispersions to the DA stars with 20 pc.

We have taken a census of DAZ and helium-rich DZ stars within 20 pc of the Sun. The DAZ stars which exhibit accreted metals and which have shorter diffusion timescales than non-DA stars, have been counted separately from the "pure" DA stars in our statistics. However, we note that there are 11 such objects or 8% of the local white dwarfs within 20 pc. Because of their short diffusion timescales, they must be accreting presently or in the very recent past. This fact coupled with the complete lack of any local interstellar clouds of sufficient density (Aannestad & Sion 1985; Aannestad et al. 1993) implies they must be accreting from circumstellar material. This has been confirmed by the detection with *Spitzer Space Telescope* of debris disks around several DAZ stars (Farihi et al. 2009, and references therein). The accretion rates required to explain their observed metal abundances are as little as 3×10^8 g s^{-1}.

The helium-rich DZ stars which typically exhibit calcium and magnesium in the optical spectra account for 7% of the 20 pc sample. They have much longer diffusion timescales (and deeper convection zones) than DAs. As cooling helium-rich white dwarfs cool below 12,000 K, helium lines can no longer be detected. Since H is the lightest element, it tends to float up to the upper layers of the photosphere. Those DZs with detected H, known as DZA stars, may also have accreted H and metals from the interstellar medium or from circumstellar debris disks. However, DZ stars contain less hydrogen in their atmospheres than what is expected if the accreted material had a solar composition. Thus, the hydrogen accretion rate must be reduced relative to that of metals in order to account for the relatively low hydrogen abundances (with respect to heavier elements) observed in DZ stars (Dufour et al. 2007). While the Dupuis et al. (1993) two-phase model of interstellar accretion onto white dwarfs cannot be ruled out completely, the cooler DZ stars do not have the strong UV radiation field needed to ionize accreting H so that a weakly magnetic, slowly rotating DZ would avoid H accretion by the propellor mechanism.

Despite the detection of debris/dust disks around some but not all metal polluted white dwarfs observed by *Spitzer*, it appears highly probable that virtually all of the DAZ stars owe their metals to circumstellar accretion. Thus, from our 20 pc census of white dwarfs, if we consider only the DAZ stars, then we estimate a lower limit percentage of at least 8% of the white dwarfs within 20 parsecs of the Sun that probably have circumstellar material (debris disks) around them. Insofar as we can regard the DAZ white dwarfs as probes of their circumstellar environments, then this would suggest a high probability that at least the same percentage should have asteroid-like minor planets and possibly even terrestrial-like rocky metallic planets. Indeed one local white dwarf G29−38 (WD2326+049) in our 20 pc sample is known to have a dusty debris disk (Zuckerman & Becklin 1987) while three white dwarfs in our 20 pc sample are in systems with confirmed extrasolar planets, WD0208−510 (K1V + DA10), WD0415−594 (K2IV + DA3.8), and WD1620−391 (G2V + DA2), although the planets in the latter three systems do not orbit the white dwarf. Furthermore, if we suppose that the DZ stars, including the DZA stars (but see Section 2), have also accreted circumstellar material (have debris disks), then summing the DZ stars with the DAZ stars, we speculate that at least 15% of the white dwarfs within 20 pc of the Sun have circumstellar debris disks with rocky, metallic debris.

We have excluded the DQ stars from this estimate. While it is possible that the DQ white dwarfs may accrete from circumstellar or even interstellar matter, we do not include them in our estimate because we regard it more likely that the source of their photospheric carbon is either due to convective mixing (Dufour et al. 2005, and references therein) or is primordial (Dufour et al. 2007). Indeed, only one DQ has been found to have atmospheric hydrogen (G99−37). Accreted metals are also easier to hide in DQ atmospheres due to the increased opacity provided by carbon.

We are grateful to an anonymous referee for numerous helpful suggestions and comments. This work was supported by NSF grant AST05-07797 to the University of Arizona, Villanova University, and the Florida Institute of Technology. Participation by TDO was also supported by NSF grant AST-0807919 to FIT.

REFERENCES

Aannestad, P. A., Kenyon, S. J., Hammond, G. L., & Sion, E. M. 1993, AJ, 105, 1033
Aannestad, P. A., & Sion, E. M. 1985, AJ, 90, 1832
Anselowitz, T., et al. 1999, PASP, 111, 702
Bahcall, J. N. 1984, ApJ, 276, 169
Chauvin, G., Lagrange, A.-M., Udry, S., & Mayor, M. 2007, A&A, 475, 723
Chiba, M., & Beers, T. 2000, AJ, 119, 2843

Davies, M. B., Kolb, U., King, A. R., & Ritter, H. 2001, in ASP Conf. Ser. 229, Evolution of Binary and Multiple Star Systems, ed. Ph. Podsiadlowski, et al. (San Francisco, CA: ASP), 443
Dufour, P., Bergeron, P., & Fontaine, G. 2005, ApJ, 627, 404
Dufour, P., Liebert, J., Fontaine, G., & Behara, N. 2007, Nature, 450, 522
Dufour, P., et al. 2007, ApJ, 663, 1291
Dupuis, J., Fontaine, G., & Wesemael, F. 1993, ApJS, 87, 345
Farihi, J., Jura, M., & Zuckerman, B. 2009, ApJ, 694, 805
Greenstein, J. 1986, ApJ, 304, 334
Holberg, J. B. 2009, J. Phys. Conf. Ser., 172, 012022
Holberg, J. B., & Bergeron, P. 2006, AJ, 132, 1221
Holberg, J. B., Bergeron, P., & Gianninas, A. 2008, AJ, 135, 1239
Holberg, J. B., Sion, E. M., Oswalt, T., Mc Cook, G. P., Foran, S., & Subasavage, J. P. 2008, AJ, 135, 1225 (LS08)
Kawaler, S. D. 1996, ApJ, 467, 61
Kawka, A., & Vennes, S. 2006, ApJ, 643, 402
Kawka, A., et al. 2006, ApJ, 643, L123
Lépine, S., Rich, R., & Shara, M. M. 2005, ApJ, 633, 121
Liebert, J. 1988, PASP, 100, 1302
Mugrauer, M., & Neuhäuser, R. 2005, MNRAS, 361, 15
Napiwotzki, R. 2006, A&A, 451, 27
Napiwotzki, R. 2009, J. Phys. Conf. Ser., 172, 012004
Oppenheimer, et al. 2001, Science, 292, 698
Oswalt, T. D., Smith, J. A., Wood, M. A., & Hintzen, P. 1996, Nature, 382, 692
Pauli, E.-M., Napiwotzki, R., Altmann, M., Heber, U., & Odenkirchen, M. 2003, A&A, 400, 877
Pauli, E.-M., Napiwotzki, R., Heber, U., Altmann, M., & U. Odenkirchen, M. 2006, A&A, 447, 173
Rappaport, S., Di Stefano, R., & Smith, J. D. 1994, ApJ, 426, 692
Silvestri, N., Oswalt, T. D., & Hawley, S. 2002, AJ, 124, 1118
Sion, E. 1984, ApJ, 282, 612
Sion, E. M., Fritz, M., McMullin, J. P., & Lallo, M. D. 1988, AJ, 96, 251
Strittmatter, P., & Wickramasinghe, D. T. 1971, MNRAS, 152, 47
Subasavage, J. P., Henry, T. J., Bergeron, P., Dufour, P., & Hambly, N. C. 2008, AJ, 136, 899
Subasavage, J., et al. 2009, AJ, 137, 4547
Wooley, R., et al. 1970, Ann. R. Obs., 5
Zuckerman, B., & Becklin, E. E. 1987, Nature, 300, 138